8-22-2022

Identification of Lithocholic Acid as a Molecular Glass Host for Room-Temperature Phosphorescent Materials

John J. Flynn

Zachary M. Marsh

Douglas M. Krein

Steven M. Wolf

Joy E. Haley

See next page for additional authors

Author(s)
John J. Flynn, Zachary M. Marsh, Douglas M. Krein, Steven M. Wolf, Joy E. Haley, Erick S. Vasquez, Thomas M. Cooper, Nicholas P. Godman, and Tod A. Grusenmeyer

ChemPhotoChem

Research Articles
doi.org/10.1002/cptc.202200134

Chemistry Europe
European Chemical Societies Publishing

www.chemphotochem.org

Identification of Lithocholic Acid as a Molecular Glass Host for Room-Temperature Phosphorescent Materials

John J. Flynn,[a, b, f] Zachary M. Marsh,[a, d] Douglas M. Krein,[a, e] Steven M. Wolf,[a, d] Joy E. Haley,[a] Erick S. Vasquez,[c] Thomas M. Cooper,[a] Nicholas P. Godman,[a] and Tod A. Grusenmeyer*[a]

Lithocholic acid was identified as a molecular glass host material for room temperature phosphorescent (RTP) chromophores. Differential scanning calorimetry (DSC) was performed on a series of structurally similar, biologically sourced molecules, including lithocholic acid, β-estradiol, cholesterol, and β-sitosterol, in an effort to identify new amorphous molecular glasses independent of plasticizing additives. DSC analysis revealed lithocholic acid and β-estradiol form stable molecular glasses post thermal processing unlike neat cholesterol and β-sitosterol. The ability of lithocholic acid and β-estradiol to stabilize high wt.% loadings of d^{10}-pyrene and a mixture of d^{10}-pyrene and an iridium chromophore, bis(2,4-difluorophenylpyridinato)-tetrakis(1-pyrazolyl)borate iridium(III) (FIr6), was also investigated. All β-estradiol formulations show β-estradiol cold crystallization. Optical microscopy and wide angle X-ray scattering measurements suggest spherulite β-estradiol crystals form during this process. Finally, time-resolved luminescence and phosphorescence quantum yield experiments show that the d^{10}-pyrene RTP lifetime is longer and the d^{10}-pyrene phosphorescence quantum yield is higher in lithocholic acid molecular glasses than in β-estradiol molecular glasses. The discrepancy in lifetime and quantum yield values is explained by quantitatively smaller rates of non-radiative decay from the triplet state of d^{10}-pyrene in lithocholic acid.

Introduction

A number of strategies have been explored to create and enhance room temperature phosphorescence (RTP) in organic materials. These include the structural engineering of pure organic luminophores,[1–5] organic aggregates,[6] amorphous polymers,[7,8] host-guest and hydrogen/halogen bonding systems,[9–11] co-crystals,[12] and organic inorganic hybrid systems.[13] RTP normally arises as a result of efficient phosphorescence from the triplet excited-states of organic chromophores.[1–4,6,8,10,11,13,14] Due to spin-forbidden relaxation of triplet excited-states, the lifetimes of triplet excited states tend to be longer (seconds to hundreds of nanoseconds) relative to those of the singlet state (tens of nanoseconds to picoseconds).[15] Many RTP materials incorporate a host system that limits diffusional oxygen quenching of the chromophore excited-state and decreases nonradiative decay (k_{nr}) in the triplet excited-state of chromophore.[16,17] RTP has been demonstrated in a number of organic host materials such as polymers,[18–20] β-cyclodextrins,[21–23] cucurbiturils,[24–28] and molecular glasses.[2,29–34] Steroidal molecular glasses have been identified as promising host materials for RTP due to their ability to serve as oxygen barriers, reduce k_{nr}, and form stable, optically transparent amorphous glasses. Hirata *et al.* have demonstrated the use of steroidal β-estradiol molecular glasses with deuterated chromophores yielding lifetimes on the order of 10^0 seconds.[16] Since then β-estradiol molecular glass hosts have been used in demonstrations ranging from reverse saturable absorption,[35–38] long-lived persistent RTP,[2,17,31–34] polarization of light,[39] and thermally activated delayed fluorescence.[17] This work attempts to identify alternative biologically sourced RTP host materials with the capacity to form stable molecular glasses.

Generally, successful glass formers have low molecular symmetry, numerous rotatable bonds, high degrees of branching, and the presence of electronegative elements such as oxygen, nitrogen, and sulfur.[40] Successful glass formers tend to have molecular weights that exceed 300 g mol^{-1}.[41] The physiochemical properties of these compounds often include a large melting enthalpy, a high melting temperature, and a low heat

[a] J. J. Flynn, Dr. Z. M. Marsh, D. M. Krein, Dr. S. M. Wolf, Dr. J. E. Haley, Dr. T. M. Cooper, Dr. N. P. Godman, Dr. T. A. Grusenmeyer
Air Force Research Laboratory
Materials and Manufacturing Directorate/
Wright-Patterson Air Force Base
Dayton, Ohio 45433 (USA)
E-mail: tod.grusenmeyer.1@us.af.mil
[b] J. J. Flynn
Strategic Ohio Council for Higher Education
Dayton, Ohio, 45440 (USA)
[c] Prof. E. S. Vasquez
Department of Chemical and Materials Engineering
University of Dayton
Dayton Ohio, 45469 (USA)
[d] Dr. Z. M. Marsh, Dr. S. M. Wolf
Azimuth Corporation
2079 Presidential Dr. #200, Fairborn, OH 45342 (USA)
[e] D. M. Krein
General Dynamics Information Technology
Dayton, Ohio 45431 (USA)
[f] J. J. Flynn
Current address:
Colorado State University
Walter Scott Jr. College of Engineering
Fort Collins, Colorado, 80523 (USA)

Supporting information for this article is available on the WWW under https://doi.org/10.1002/cptc.202200134

of fusion (ΔH_{fus}).[42] Although these criteria are not universal, small molecules that meet a majority of these rules tend to undergo vitrification without crystallization. The commonly used glass forming steroid, β-estradiol, has an unsymmetrical hydrocarbon core containing high degrees of branching, multiple hydroxyl moieties, and has a melting point of 168 °C. However, β-estradiol has a molecular weight under 300 g mol^{-1} and still forms a stable amorphous glass without crystallization. The steroid cholesterol is highly asymmetrical, contains a highly branched hydrocarbon core, has a molecular weight exceeding 300 g mol^{-1}, contains a hydroxyl moiety, and has a melting point of 150 °C. It does not form an amorphous glass without crystallite development during thermal processing. Though these design rules are useful and aid in determining alternative host materials, the complex nature of vitrification stresses the need for extensive thermal characterization of any potential host material.

The vitrification behavior of many molecular glass hosts is further complicated by the addition of a guest molecule which can influence the thermal behavior of the host and induce crystallization. This is especially relevant for RTP materials as the guest molecules are often rigid polycyclic aromatic hydrocarbons (PAHs). Thermal studies of small molecules containing rigid aromatic moieties have shown these materials readily undergo hot crystallization in neat melts.[40] It has also been shown that rigid aromatic guests can induce crystallization of the host glass,[43] sublime or evaporate during thermal processing,[44] and/or form aggregates in the glass.[45,46] Therefore, the amorphous host must be able to maintain dispersion of the guest. This again stresses the need for extensive thermal characterization of potential molecular glass hosts in the presence of the guest to obtain a thorough understanding of a host-guest formulation's thermal and vitrification behavior.

This work describes the use of differential scanning calorimetry (DSC) to characterize the thermal properties of four structurally similar biologically sourced molecules, β-estradiol, lithocholic acid, cholesterol, β-sitosterol, in order to evaluate their suitability as molecular glass hosts for RTP chromophores.[47] This analysis shows that lithocholic acid and β-estradiol form stable molecular glasses in neat form and in the presence of high wt.% loadings of d-10 pyrene. Similarly, both materials form a stable glass with a mixture of d^{10}-pyrene and an iridium chromophore, Bis(2,4-difluorophenylpyridinato)-tetrakis(1-pyrazolyl)borate iridium (III) (FIr6). Photoluminescence experiments show that the RTP lifetime of d^{10}-pyrene is longer and the phosphorescence quantum yield of d^{10}-pyrene is greater in lithocholic acid molecular glasses than in β-estradiol molecular glasses. A detailed discussion of the thermal properties of the neat biologically sourced molecules, the thermal properties of host-guest formulations containing d^{10}-pyrene and d^{10}-pyrene with FIr6 in lithocholic acid and β-estradiol, the preparation of molecular glass thin-films, and steady-state and time-resolved phosphorescence experiments are presented within.

Results and Discussion

Thermal bounds for the heating and cooling cycles were selected *via* a 2 wt.% loss in Thermal Gravimetric Analysis (TGA) profiles attributed to degradation of the steroidal host materials as shown in Figure S1. Evidence of water loss was commonly observed around 100 °C for all steroidal hosts except lithocholic acid, and the flat line formed after water effluence was taken as the baseline to determine 2 wt.% loss. An upper temperature bound of 200 °C was selected as no mass loss was observed and melting temperatures for all steroidal hosts were expected below this temperature. DSC allows for the identification of the melting point (T_m), glass transition temperature (T_g), cold crystallization temperature (T_{cc}), and the enthalpy of melt (ΔH_m) of a given material. For a compound to qualify as a host material, it must form an amorphous glass after thermal processing. Thus, the material should exhibit a transition into an amorphous glass without the presence of crystallization peaks from the neat melt during cooling.[48] While molecular glasses supplemented with plasticizing agents to reduce crystallite formation have been demonstrated for steroidal hosts in previous studies, the objective of this study is to identify amorphous glass hosts independent of plasticizing additives.[49] The chemical structures of the four biologically sourced molecules β-estradiol, lithocholic acid, cholesterol, and β-sitosterol as well as the chromophores d^{10}-pyrene and FIr6 are shown in Figure 1.

Thermal Analysis of Biologically Sourced Molecules

DSC traces of neat β-estradiol, lithocholic acid, cholesterol, and β-sitosterol are shown in Figure 2. Insets highlighting glass transitions are provided. Tables S1 and S2 contain T_g, T_m, and ΔH_m values obtained for each of the molecules. Both β-estradiol and lithocholic acid form stable amorphous molecular glasses from the melt as a glass transition is observable with no crystallization peaks during cooling. In β-estradiol (Figure 2, top left), a melting peak at 179 °C was observed followed by a glass transition at 82 °C during cooling. During the second heating cycle an exothermic feature at 131 °C is observed, indicating cold crystallization of the β-estradiol suggesting some nuclei are formed during cooling and the cooling rate is fast enough to suppress crystal growth.[48] Lithocholic acid (Figure 2, top right) exhibits a sharp melting peak at 186 °C during the first heating cycle followed by a glass transition at 84 °C during cooling. Lithocholic acid does not exhibit a cold crystallization peak during the second heating cycle. Cholesterol (Figure 2, bottom left) exhibits a melting peak at 147 °C during the first heating cycle followed by crystallization peaks at 115 °C and 20 °C during the first cooling cycle. No glass transition is observed during thermal cycling of cholesterol. β-sitosterol (Figure 2, bottom right) displays a melting peak at 134 °C during the first heating cycle. This is followed by a prominent crystallization peak at 120 °C in the first cooling cycle. Similar to cholesterol, no glass transition was observed for β-sitosterol,

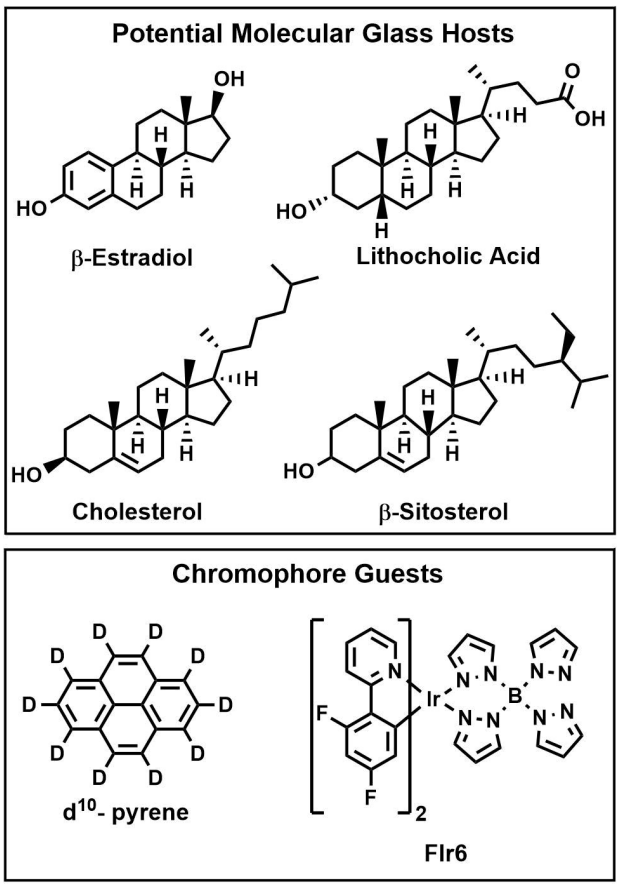

Figure 1. Chemical structures of biologically sourced molecules evaluated as molecular glass host materials and guest chromophores.

indicating that neither cholesterol nor β-sitosterol forms an amorphous glass from the neat melt.

Two trends are apparent when comparing the thermal properties of the four neat steroids and their vitrification behavior. First, a trend in ΔH_m is observed with β-estradiol having the highest melting enthalpy of 112.5 J/g followed by lithocholic acid at 97.2 J/g, cholesterol at 77.3 J/g, and β-sitosterol at 52.4 J/g. A trend is also observed for T_m with lithocholic acid (187.1 °C) having the highest melting temperature followed by β-estradiol (179.1 °C), cholesterol (147.9 °C), and β-sitosterol (136.7 °C). Both ΔH_m and T_m have been cited as important factors that impact the vitrification behavior of a material. Compounds with higher melting enthalpies and temperatures often form amorphous glasses while compounds with lower melting enthalpies and temperatures often crystallize during the cooling cycle disrupting glass formation.[42,50] A significant observation from the thermal analysis of the four host materials is that ΔH_m and T_m are both higher in the two amorphous glass forming hosts, lithocholic acid and β-estradiol, than in the two non-glass forming hosts, cholesterol and β-sitosterol. Hereafter, we will limit our discussion to host-guest molecular glasses utilizing lithocholic acid and β-estradiol.

X-Ray Scattering Analysis and Optical Microscopy Images of Cold Crystallization in β-Estradiol

Wide angle X-ray Scattering (WAXS) diffraction patterns were collected for neat β-estradiol and the amorphous glass formed after thermal processing. WAXS patterns collected on a neat β-estradiol molecular glass thin-film and temperatures ranging from 155–220 °C and an optical microscopy image of β-estradiol spherulite formation during the cold crystallization process are shown in Figure 3.

Neat β-estradiol powder exhibits numerous crystalline peaks that are most consistent with the estradiol anhydrate crystal structure,[51] as shown in Figure S11. After thermal processing of the neat powder an amorphous glass phase is obtained, this is supported by the broad amorphous peak observed in the WAXS pattern of Figure S12. These results are consistent with the DSC thermal analysis of neat β-estradiol shown in Figure S4. Temperature dependent WAXS experiments were performed to elucidate the cold crystallization process. As the amorphous glass is heated above the cold crystallization temperature the broad amorphous peak is replaced by defined scattering features similar to the neat powder. As the temperature is increased further the peaks become more defined suggesting continued growth of the β-estradiol crystallites. Once the sample is heated above the melting temperature, the defined scattering peaks are replaced by a small broad feature that is attributed to the β-estradiol melt. The temperature dependent WAXS pattern of β-estradiol exhibits some peaks consistent with the estradiol anhydrate crystal structure as shown in Figure S12. However, numerous peaks in the WAXS pattern are inconsistent with the anhydrate crystal suggesting a different crystal structure is forming. An optical microscopy image is provided in Figure 3 showing the growth of spherulite crystals above the cold crystallization temperature of β-estradiol. This leads to the conclusion that the unique scattering patterned observed in our temperature dependent WAXS measurements arrive from β-estradiol spherulite crystal scattering.

Thermal Analysis of Lithocholic Acid and β-Estradiol Host–Guest Molecular Glasses with d^{10}-Pyrene

The chromophore chosen for incorporation with the steroidal hosts was the polycyclic aromatic hydrocarbon d^{10}-pyrene. Host-guest formulations commonly employ d^{10}-pyrene due to its sufficient phosphorescence quantum yield and long phosphorescence lifetime.[35,52] DSC analysis was performed on neat d^{10}-pyrene prior to the incorporation of the chromophore into lithocholic acid and β-estradiol molecular glass hosts. DSC traces of d^{10}-pyrene are shown in Figure S2. Samples of d^{10}-pyrene exhibit crystallization upon thermal cycling. A melting peak is observed at 151 °C during the first heating cycle with rapid crystallization occurring during the first cooling cycle at 125 °C. Hysteresis of the crystallization peak was observed for both thermal cycles due to rapid crystallization rates and self-heating within the sample.[53]

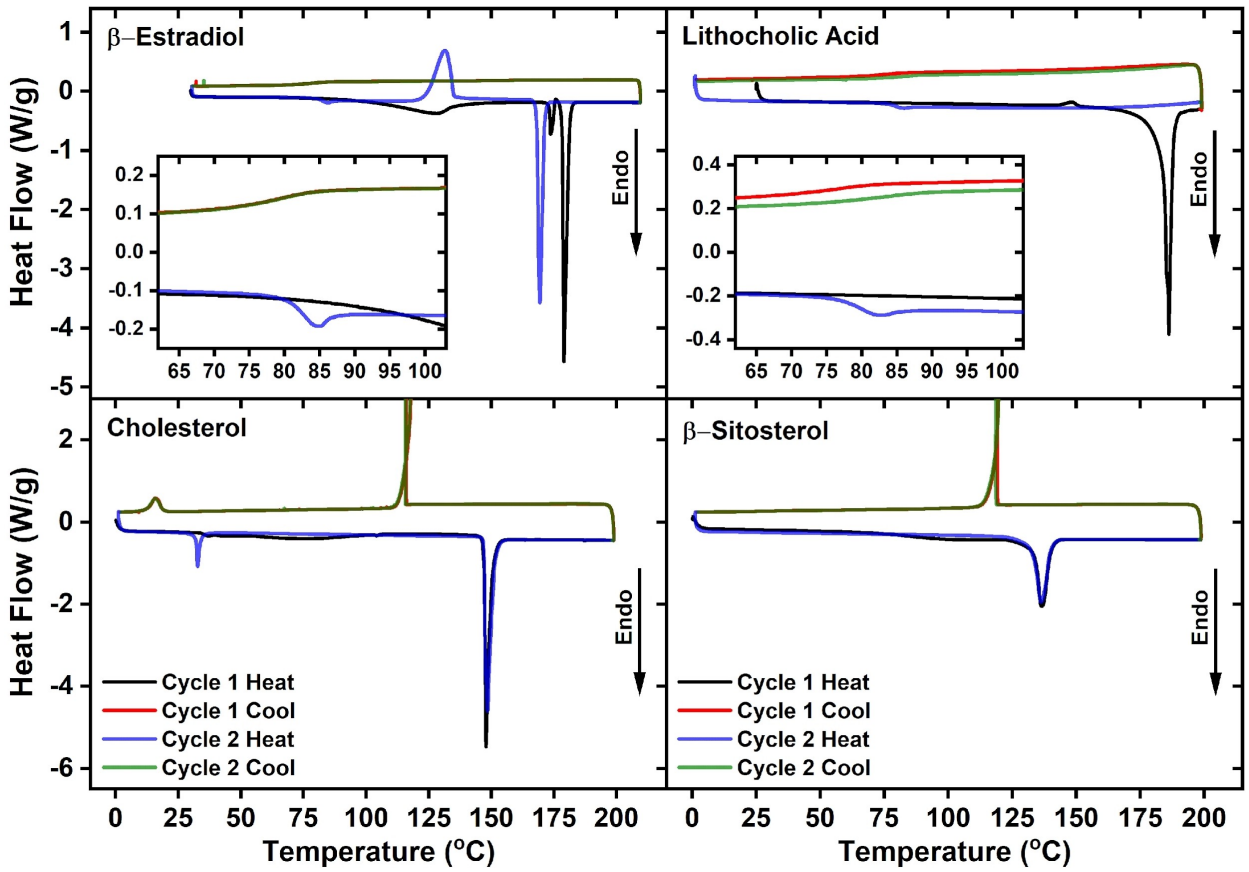

Figure 2. Differential scanning calorimetry of potential host materials (top left) β-estradiol, (top right) lithocholic acid, (bottom left) cholesterol, and (bottom right) β-sitosterol. Insets show glass transitions and endothermic features attributed to molecular relaxation for β-estradiol and lithocholic acid. The first heating cycle is depicted in black, the first cooling cycle is depicted in red, the second heating cycle is depicted in blue, and the second cooling cycle is depicted in green.

Following the thermal characterization of neat d^{10}-pyrene, the thermal properties of lithocholic acid and β-estradiol in the presence of increasing d^{10}-pyrene loading were explored. The DSC traces obtained for neat samples of lithocholic acid and β-estradiol as well as the host-guest formulations with 8 wt.% d^{10}-pyrene loadings are shown in Figure 4. DSC traces of lithocholic acid and β-estradiol containing 1 wt.% and 3 wt.% loadings of d^{10}-pyrene are shown in Figures S3 and S4, respectively. Table S1 & S2 summarize the T_g, T_m, and ΔH_m values for all lithocholic acid and β-estradiol host-guest formulations. Each lithocholic acid and d^{10}-pyrene formulation shows a melting peak for d^{10}-pyrene at 151 °C and a melting peak for lithocholic acid between 179–185 °C during the initial heating cycle. Each formulation exhibits a T_g between 67–75 °C. Host-guest formulations containing lithocholic acid and d^{10}-pyrene do not exhibit any signs of guest crystallization following glass formation and no melting peaks attributable to d^{10}-pyrene on the second heating cycle were observable. For β-estradiol and d^{10}-pyrene formulations, melting peaks corresponding to d^{10}-pyrene at 151 °C and β-estradiol between 176–179 °C were observed during the initial heating cycle. Each formulation exhibits a T_g between 75–82 °C. These formulations also show a cold crystallization peak at temperatures ranging from 133–139 °C during the second heating cycle attributed to β-estradiol. A d^{10}-pyrene melting peak at 154 °C is also present during the second heating cycles of all β-estradiol and d^{10}-pyrene formulations. The melt enthalpy associated with d^{10}-pyrene increases as the wt.% loading of d^{10}-pyrene increases. The observation of a d^{10}-pyrene melting peak during the second heating cycle suggests that d^{10}-pyrene also crystallizes during the cold crystallization of β-estradiol.

Three trends are apparent when analyzing T_g, ΔH_m, and T_m as a function of d^{10}-pyrene loading in host-guest formulations of lithocholic acid and d^{10}-pyrene and β-estradiol and d^{10}-pyrene. The first trend is a monotonic reduction in the T_g as d^{10}-pyrene loading is increased. In lithocholic acid, the T_g decreases from 75.1 °C for the neat melt to 67.1 °C for the highest d^{10}-pyrene loading. Host-guest samples of β-estradiol containing d^{10}-pyrene exhibit a similar decrease in the T_g from 82.4 °C for the neat melt to 75.2 °C for the highest d^{10}-pyrene loading. Fluctuations in ΔH_m are observed for both host-guest formulations. An 18.06% change in ΔH_m from 87.5 to 71.7 J/g is observed for lithocholic acid as the loading of d^{10}-pyrene increases from 1.5 to 8.2%. In β-estradiol a much more significant change of 63.27% in ΔH_m from 76.5 to 28.1 J/g is observed as the loading of d^{10}-pyrene increases from 1.2 to 8.0%. Both lithocholic acid and β-estradiol show a monotonic decrease in T_m as the wt.% loading of d^{10}-pyrene is increased.

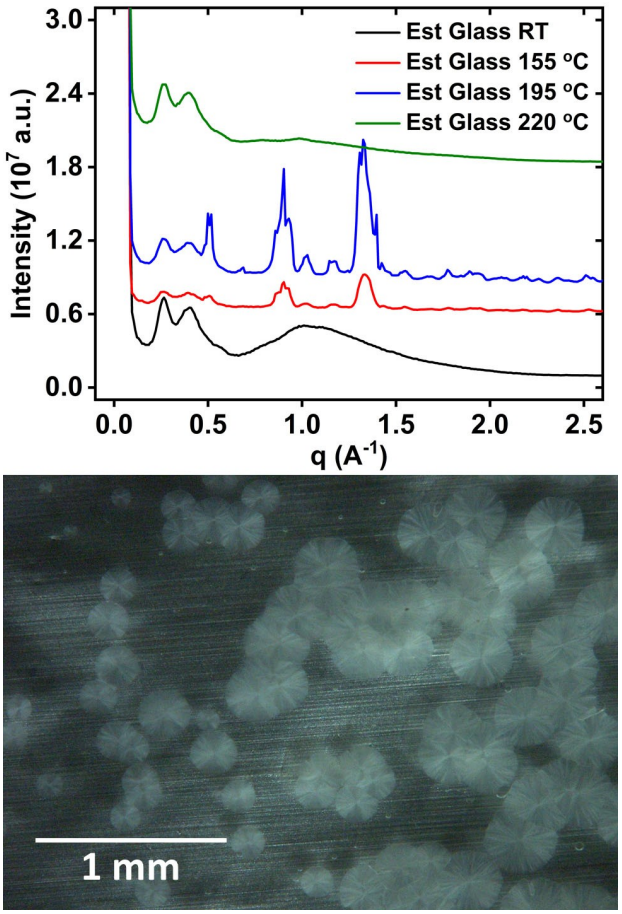

Figure 3. (Top) Temperature dependent WAXS patterns of the β-estradiol glass showing the formation of crystallites as the material is heated above the cold crystallization temperature followed by complete melting of the β-estradiol. (Bottom) Optical microscopy image of β-estradiol spherulite formation during the cold crystallization process. Image collected at 135 °C.

Thermal Analysis of Lithocholic Acid and β-estradiol Host–Guest Molecular Glasses with FIr6 and d^{10}-Pyrene

Finally, the thermal properties of host-guest formulations containing mixtures of FIr6 and d^{10}-pyrene in lithocholic acid and β-estradiol were investigated. Interest in these formulations is driven by donor-acceptor photochemistry that allows for visible light rather than UV light excitation of the long-lived d^{10}-pyrene triplet state.[35,37,38] For each host-guest formulation, the loading of d^{10}-pyrene was held constant at 5.0 wt.% while FIr6 loading was increased from 1.0–5.0 wt.%. Representative DSC traces of lithocholic acid loaded with 5.4 wt.% d^{10}-pyrene and 3.0 wt.% FIr6 as well as β-estradiol loaded with 5.5 wt.% d^{10}-pyrene and 2.7 wt.% FIr6 are shown in Figure 5. DSC traces for lithocholic acid and β-estradiol with 5 wt.% d^{10}-pyrene and increasing FIr6 loading are presented in Figures S5 and S6, respectively. Tables S1 and S2 contain the T_g, T_m, and ΔH_m values for the FIr6 and d^{10}-pyrene formulations.

The DSC behavior of lithocholic acid and β-estradiol formulations containing FIr6 and d^{10}-pyrene are similar to the lithocholic acid and β-estradiol formulations containing only d^{10}-pyrene. Each lithocholic acid formulation shows a melting peak for d^{10}-pyrene at 151 °C and a melting peak for lithocholic acid near 181 °C during the initial heating cycle. Each lithocholic acid formulation exhibits a T_g of approximately 70 °C. Host-guest formulations in lithocholic acid do not exhibit signs of guest crystallization following lithocholic acid glass formation and no melting peaks attributable to d^{10}-pyrene on the second heating cycle are observed. For β-estradiol formulations a melting peak corresponding to d^{10}-pyrene at 151 °C with a melting peak for β-estradiol near 176 °C during the initial heating cycle is observed. Each β-estradiol formulation exhibits Tg values close to 75 °C. These formulations also show a cold crystallization peak at approximately 140 °C during the second heating cycle attributed to β-estradiol. A d^{10}-pyrene melting peak is also observed at 154 °C during the second heating cycle of all β-estradiol formulations. The melt enthalpy associated with d^{10}-pyrene increases as the wt.% loading of d^{10}-pyrene increases. Again, this observation of a d^{10}-pyrene melting peak during the second heating cycle suggests that d^{10}-pyrene also crystallizes during the cold crystallization of β-estradiol.

The observed trends in T_g, ΔH_m, and T_m as a function of FIr6 loading in lithocholic acid and β-estradiol molecular glasses containing a mixture FIr6 and d^{10}-pyrene are similar to those observed in host-guest formulations containing only d^{10}-pyrene. A small depression in the T_g is observed in both lithocholic acid and β-estradiol molecular glasses as the FIr6 loading is increased. The magnitude of ΔH_m also decreases in both lithocholic acid and β-estradiol molecular glasses as the FIr6 loading is increased. The ΔH_m for lithocholic acid decreases from 97.2 to 76.3 J/g upon loading with 5.0 wt.% FIr6 and 4.7 wt.% d^{10}-pyrene while the ΔH_m for β-estradiol decreases from 90.7 J/g for the neat melt to 50.0 J/g for the formulation containing 4.7 wt.% FIr6 and 5.6 wt.% d^{10}-pyrene, respectively. Both lithocholic acid and β-estradiol molecular glass formulations also show a slight reduction in the T_m as the FIr6 loading is increased.

Thin-Film Sample Preparation, Ground State Absorption, and Room Temperature Phosphorescence (RTP)

The luminescent properties of neat d^{10}-pyrene and mixtures of d^{10}-pyrene and FIr6 in lithocholic acid and β-estradiol were compared. All molecular glass samples were cast between glass slides cleaned in a plasma chamber. Glass slides with dimensions of 3.8 cm × 2 cm were used for all luminescence measurements. Molecular glass thin-films were prepared by melting solid powders on a glass slide prior to the second slide being added on top of the melted solids. While in the melt phase, the glass slides were depressed to force air bubbles out of the films. The films were then rapidly cooled by removal from the heat source followed by placing the sample on an aluminum block. This process was repeated until thin-films of high optical clarity were obtained. Photos depicting the thin-film melt process and typical molecular glass samples are shown in Figures S7 and S8. The thickness of the molecular glass thin-films was measured using a digital indicator with a spindle lifting cable relative to a flat surface. The thickness was

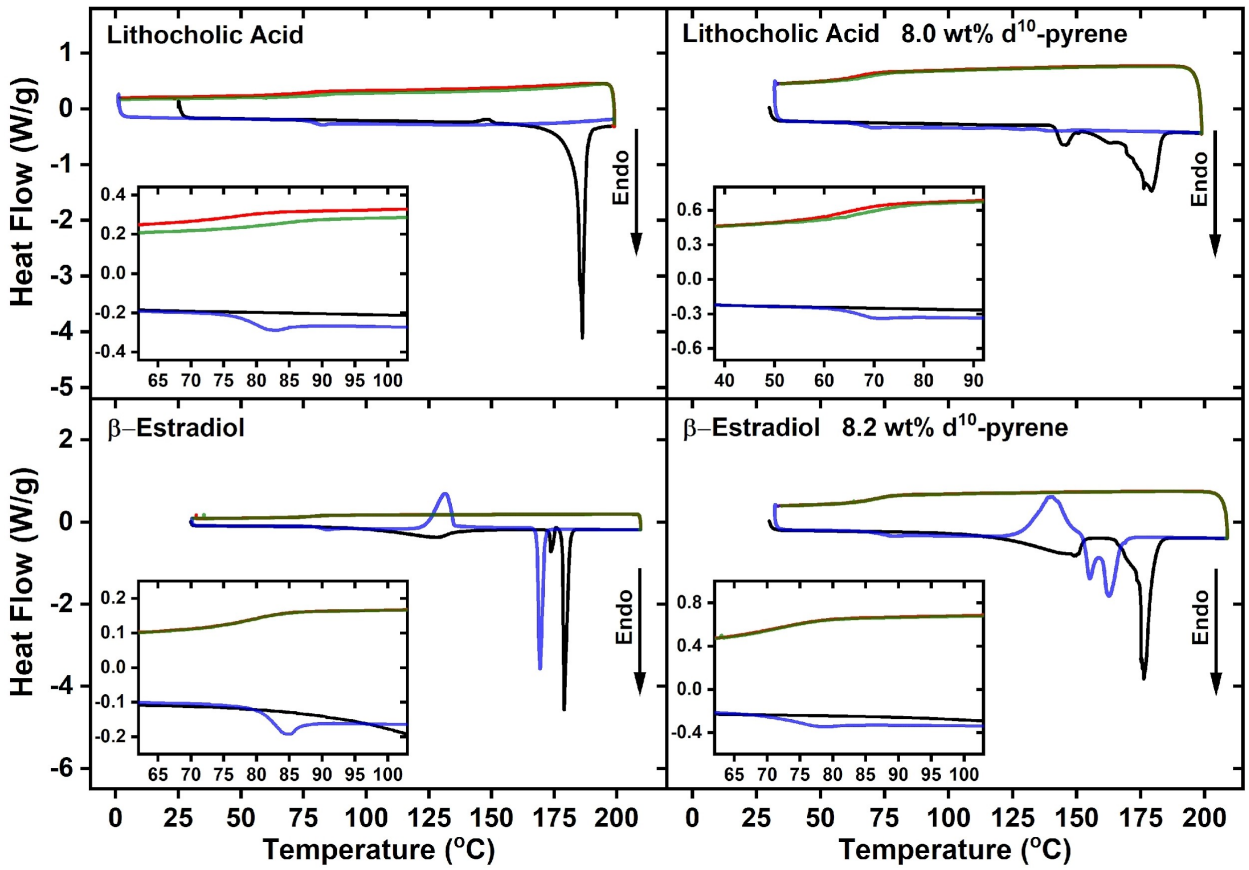

Figure 4. Differential scanning calorimetry of (top left) lithocholic acid, (top right) lithocholic acid loaded with 8.0 wt.% d^{10}-pyrene, (bottom left) β-estradiol, and (bottom right) β-estradiol with 8.2 wt.% d^{10}-pyrene. Insets show glass transitions and endothermic features attributed to molecular relaxation for β-estradiol and lithocholic acid. The first heating cycle is depicted in black, the first cooling cycle is depicted in red, the second heating cycle is depicted in blue, and the second cooling cycle is depicted in green.

recorded by measuring the four corners of a glass coupon and averaging the thickness values. A box and whisker plot showing the range in thickness across the films is shown in Figure S9. Lithocholic acid films had a mean thickness of 63 μm while β-estradiol films had a mean thickness 71 μm. The range of measured thickness values was greater for β-estradiol films (Q_1–Q_3 range: 54–80 μm) than lithocholic acid films (Q_1–Q_3 range: 57–68 μm).

The ground-state absorption spectra of samples containing 5 wt.% d^{10}-pyrene in lithocholic acid and β-estradiol as well as 1 wt.% Flr6 and 5 wt.% d^{10}-pyrene in lithocholic acid and β-estradiol are shown in Figure S10. The ground-state absorption spectra of the samples are dominated by a strong π-π* UV absorption from d^{10}-pyrene. Smaller absorption peaks are observed at 363 nm and 372 nm in each of the samples. These peaks are attributed to the weak S_0 to S_1 π-π* transition in pyrene.[15] The increase in absorption at wavelengths shorter than 350 nm and the tailing absorption at wavelengths longer than 400 nm in 1 wt.% Flr6 and 5 wt.% d^{10}-pyrene samples is ground-state absorption from the Flr6 complex. Irradiation of d^{10}-pyrene – Flr6 samples at 405 nm should result only in the direct excitation of Flr6. Any d^{10}-pyrene phosphorescence will come as a result of a Flr6-to-d^{10}-pyrene energy transfer process. The ground-state absorption features of d^{10}-pyrene remain well-resolved and there is no evidence of low energy absorption transitions at 5 wt.% pyrene loading. This suggests that there is no aggregate formation in these thin-films.[54] Given the similar average thickness values in lithocholic acid and β-estradiol thin-films, we believe the multiple melt technique results in relatively uniform distribution of the guest chromophores due to similar absorbance values obtained in the lithocholic acid and β-estradiol thin-films.

Steady-state and time-resolved luminescence measurements were performed on lithocholic acid and β-estradiol glasses containing 2 wt.% d^{10}-pyrene, 3 wt.% d^{10}-pyrene, and 5 wt.% d^{10}-pyrene as well as lithocholic acid and β-estradiol glasses containing 1 wt.% Flr6 and 5 wt.% d^{10}-pyrene. Gated phosphorescence intensity spectra and phosphorescence lifetime decays collected on lithocholic acid and β-estradiol glasses containing 5 wt.% d^{10}-pyrene as well as lithocholic acid and β-estradiol glasses containing 1 wt.% Flr6 and 5 wt.% d^{10}-pyrene are shown in Figure 6. Phosphorescence quantum yields, phosphorescence lifetimes, and the radiative and non-radiative decay rate constants for lithocholic acid and β-estradiol glasses containing 2 wt.% d^{10}-pyrene, 3 wt.% d^{10}-pyrene, and 5 wt.% d^{10}-pyrene are presented in Table 1. Steady-state intensity spectra and phosphorescence lifetime decays collected on lithocholic acid and β-estradiol glasses containing 2 wt.% d^{10}-

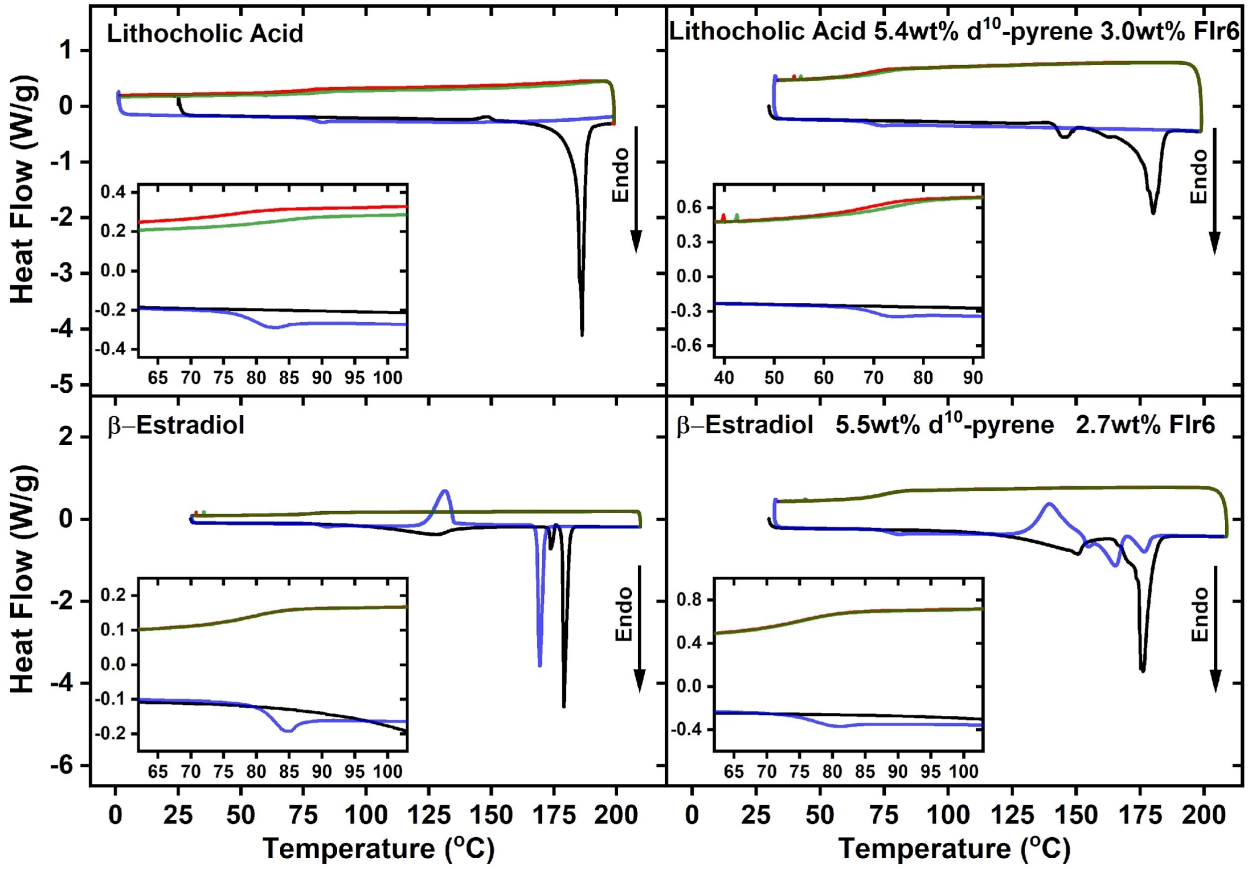

Figure 5. Differential scanning calorimetry of (top left) lithocholic acid, (top right) lithocholic acid loaded with 5.4 wt.% d^{10}-pyrene and 3.0 wt.% Flr6, (bottom left) β-estradiol, and (bottom right) β-estradiol with 5.5 wt.% d^{10}-pyrene and 2.7 wt.% Flr6. Insets show glass transitions and endothermic features attributed to molecular relaxation for β-estradiol and lithocholic acid. The first heating cycle is depicted in black, the first cooling cycle is depicted in red, the second heating cycle is depicted in blue, and the second cooling cycle is depicted in green.

Table 1. Photophysical data for lithocholic acid and β-estradiol glasses containing 2 wt.% d^{10}-pyrene, 3 wt.% d^{10}-pyrene, and 5 wt.% d^{10}-pyrene.[a]

β-estradiol Sample	Phosphorescence QY[b] (Φ_p)	Phosphorescence Lifetime[c] (τ_p; seconds)	k_r [s^{-1}]	k_{nr} [s^{-1}]
2 wt% d^{10}-pyrene	0.030	2.02	0.0149	0.480
3 wt% d^{10}-pyrene	0.028	2.02	0.0139	0.481
5 wt% d^{10}-pyrene	0.022	1.61	0.0137	0.607
Lithocholic acid Sample	**Phosphorescence QY[b] (Φ_p)**	**Phosphorescence Lifetime[c] (τ_p; seconds)**	**k_r [s^{-1}]**	**k_{nr} [s^{-1}]**
2 wt% d^{10}-pyrene	0.038	2.45	0.0155	0.393
3 wt% d^{10}-pyrene	0.032	2.38	0.0134	0.407
5 wt% d^{10}-pyrene	0.033	2.20	0.0150	0.440

[a] All d^{10}-pyrene samples were excited at 355 nm. Phosphorescence lifetimes were collected with the emission monochromator wavelength set to 590 nm. [b] Phosphorescence quantum yield values were obtained using an integrating sphere. See Experimental Section for details. [c] Phosphorescence lifetimes were collected using a gate delay of 20 μs. See Experimental Section for further details.

pyrene, 3 wt.% d^{10}-pyrene, and 5 wt.% d^{10}-pyrene are shown in Figures S13–S16.

The lithocholic acid and β-estradiol glasses containing 2 wt.% d^{10}-pyrene, 3 wt.% d^{10}-pyrene, and 5 wt.% d^{10}-pyrene exhibit dual luminescence; steady-state luminescence intensity measurements (Figures S13 and S14) clearly show structured, d^{10}-pyrene π-π* fluorescence spanning from 350–550 nm and d^{10}-pyrene π-π* room temperature phosphorescence spanning from 550–800 nm.[52] The band shape of the luminescence spectra collected on the β-estradiol glass containing 5 wt.% d^{10}-pyrene is different than the other samples. A broad, structure less shoulder is apparent on the red edge (450–550 nm) of the d^{10}-pyrene π-π* fluorescence spectra. This is consistent with emission from pyrene aggregates.[55] The identity of the

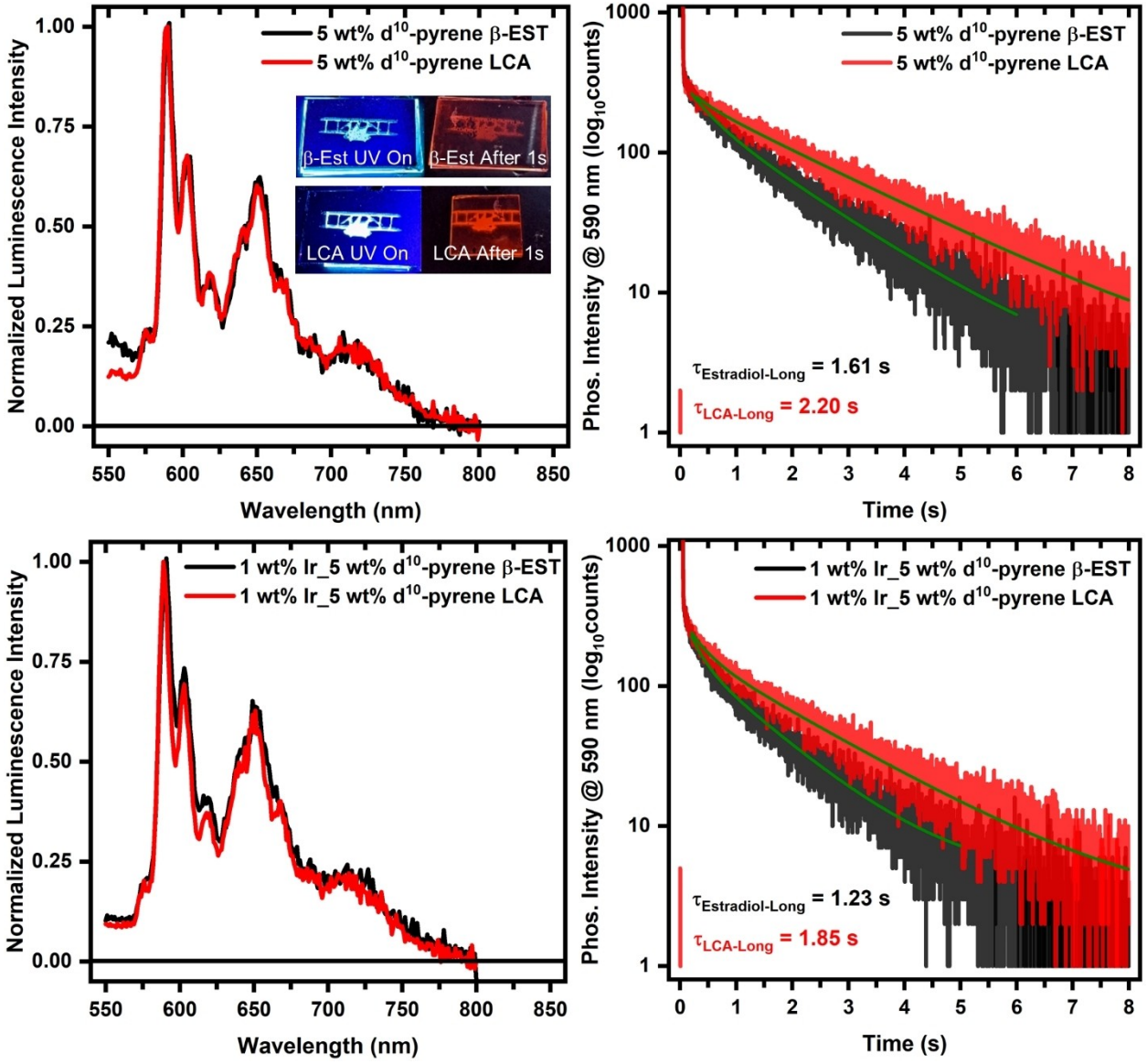

Figure 6. Steady-state luminescence spectra of 5 wt.% d^{10}-pyrene in lithocholic acid and β-estradiol (top left) and 1 wt.% FIr6 and 5 wt.% d^{10}-pyrene in lithocholic acid and β-estradiol (bottom left) and luminescence lifetimes of 5 wt.% d^{10}-pyrene in lithocholic acid and β-estradiol (top right) and 1 wt.% FIr6 and 5 wt.% d^{10}-pyrene in lithocholic acid and β-estradiol (bottom right). 5 wt.% d^{10}-pyrene samples were excited at 355 nm while 1 wt.% FIr6 and 5 wt.% d^{10}-pyrene samples were excited at 405 nm. Steady-state luminescence spectra were collected using gated detection. Phosphorescence lifetimes were collected with the emission monochromator set to 590 nm. See Experimental section for details. Inset shows β-estradiol and lithocholic acid thin-films containing 5 wt.% d^{10}-pyrene under irradiation from a UV hand lamp and one second after illumination.

molecular glass host influences both the phosphorescence quantum yield and phosphorescence lifetime in lithocholic acid and β-estradiol glasses containing 2 wt.% d^{10}-pyrene, 3 wt.% d^{10}-pyrene, and 5 wt.% d^{10}-pyrene. The phosphorescence quantum yield (Φ_P) values and phosphorescence lifetime (τ_p) values obtained from lithocholic acid glasses containing d^{10}-pyrene are quantitatively higher than those obtained from β-estradiol glasses containing d^{10}-pyrene. The collection of both the phosphorescence quantum yield and phosphorescence lifetime data allows for the calculation of the radiative (k_r) and non-radiative (k_{nr}) decay rate constants for the d^{10}-pyrene triplet excited state in lithocholic acid and β-estradiol glasses. The magnitude of the radiative decay rate constant (average value $= 0.0144 \pm 0.0008$) is similar in all six molecular glass samples containing d^{10}-pyrene while the magnitude of the non-radiative decay rate constant is quantitatively larger in β-estradiol glasses containing d^{10}-pyrene. A possible explanation for this discrepancy in the magnitude of the non-radiative decay rate constant is the structural differences between lithocholic acid and β-estradiol, particularly lithocholic acid is completely saturated while β-estradiol contains an aromatic ring.

The attributes of the decay kinetics are also impacted by the weight percent loading of d^{10}-pyrene in lithocholic acid and β-estradiol glasses containing 2 wt.% d^{10}-pyrene, 3 wt.% d^{10}-pyrene, and 5 wt.% d^{10}-pyrene (Figures S15 and S16). The initial

fast decay in all samples is attributed to the instrument response function of the spectrometer. The phosphorescence lifetime decays obtained from lithocholic acid and β-estradiol glasses containing 2 wt.% d^{10}-pyrene and 3 wt.% d^{10}-pyrene are fit well with monoexponential decay kinetics. On the other hand, the phosphorescence lifetime decays obtained from lithocholic acid and β-estradiol glasses containing 5 wt.% d^{10}-pyrene are best described by biexponential decay kinetics. The fit details obtained from biexponential fits of the lifetime decays are given in Table S3. Both the magnitude ($\tau_{SHORT,\ \beta\text{-estradiol}} = 0.42$ s) and pre-exponential contribution ($A_{SHORT,\ \beta\text{-estradiol}} = 130.2$) from the short component are greater in β-estradiol than the magnitude ($\tau_{SHORT,\ lithochlic\ acid} = 0.33$ s) and pre-exponential contribution ($A_{SHORT,\ lithochlic\ acid} = 63.9$) of the short lifetime component in lithocholic acid. The biexponential decay kinetics in these molecular glass samples is likely due to aggregate formation as broad, structure less emission is observed in β-estradiol glasses containing 5 wt.% d^{10}-pyrene.[55] The short component of the phosphorescence lifetime decay in lithocholic acid glasses containing 5 wt.% d^{10}-pyrene accounts for less than 5% of the overall decay (Table S3). This relatively small contribution to the overall excited state decay is a plausible explanation for a lack of broad, structure less emission in lithocholic acid glasses containing 5 wt.% d^{10}-pyrene. The presence of aggregates in both lithocholic acid and β-estradiol glasses containing 5 wt.% d^{10}-pyrene is further supported by a quantitative increase in the magnitude of k_{nr} in these formulations. Inclusion of the FIr6 in the molecular glass influences the phosphorescence lifetime of d^{10}-pyrene. The magnitude of the lifetime is shorter and the biexponential character of the decay is enhanced in lithocholic acid and β-estradiol molecular glasses containing FIr6. In samples containing a mixture of 5 wt.% d^{10}-pyrene and 1 wt.% FIr6, the long lifetime component of the lithocholic acid fit ($\tau_{LONG,\ lithochlic\ acid} = 1.9$ s) is again longer than the long lifetime component of the β-estradiol fit ($\tau_{LONG,\ \beta\text{-estradiol}} = 1.2$ s); however, these values represent a decrease of 15% and 33% relative to the samples containing only d^{10}-pyrene. The magnitude ($\tau_{SHORT,\ \beta\text{-estradiol}} = 0.23$ s) and pre-exponential contribution ($A_{SHORT,\ \beta\text{-estradiol}} = 178.4$) from the short component are also smaller in the d^{10}-pyrene – FIr6 β-estradiol thin-films than the magnitude ($\tau_{SHORT,\ lithochlic\ acid} = 0.32$ s) and pre-exponential contribution ($A_{SHORT,\ lithochlic\ acid} = 136.0$) in d^{10}-pyrene – FIr6 lithocholic acid thin-films. Interpretation of the FIr6 results are complicated by strong FIr6 emission from 450–650 nm (Figure S17). This obscures the collection of phosphorescence quantum yield data and the observation of pyrene aggregates from 450–550 nm. A conceivable explanation for the enhanced biexponential character in the FIr6 containing samples is inclusion of FIr6 in the molecular glass formulation increases d^{10}-pyrene aggregation.

Conclusions

DSC was used to analyze the thermal behavior of lithocholic acid, cholesterol, β-sitosterol, and the known molecular glass former, β-estradiol. Lithocholic acid was also found to form stable molecular glasses upon thermal cycling. Neat lithocholic acid samples do not exhibit signs of cold crystallization during thermal cycling while significant cold crystallization is observed for β-estradiol. The DSC behavior of lithocholic acid and β-estradiol formulations containing FIr6 and d^{10}-pyrene are similar to the lithocholic acid and β-estradiol formulations containing only d^{10}-pyrene. Each lithocholic acid formulation shows a melting peak for d^{10}-pyrene and a melting peak for lithocholic acid during the initial heating cycle. Host-guest formulations containing lithocholic acid do not exhibit any signs of crystallization following lithocholic acid glass formation and these samples have no observable melting peaks attributable to d^{10}-pyrene on the second heating cycle. Each β-estradiol formulation shows a melting peak corresponding to d^{10}-pyrene with a melting peak for β-estradiol during the initial heating cycle. All β-estradiol formulations show a cold crystallization during the second heating cycle. Optical microscopy and wide angle x-ray scattering measurements suggest spherulite β-estradiol crystals form during this process. A d^{10}-pyrene melting peak is observed along with the β-estradiol cold crystallization, suggesting that d^{10}-pyrene also crystallizes during the cold crystallization of β-estradiol. The RTP behavior of lithocholic acid and β-estradiol molecular glasses containing d^{10}-pyrene or a mixture of d^{10}-pyrene with FIr6 show that the RTP lifetime of d^{10}-pyrene in lithocholic acid molecular glasses is 40–50% longer than in β-estradiol molecular glasses. The phosphorescence quantum yield of d^{10}-pyrene is also found to be greater in lithocholic acid glasses than in β-estradiol molecular glasses. The d^{10}-pyrene lifetime decays in both molecular glass hosts loaded with 2 wt.% d^{10}-pyrene and 3 wt.% d^{10}-pyrene are best fit with monoexponential decay kinetics. The d^{10}-pyrene lifetime decays in both molecular glass hosts loaded with 5 wt.% d^{10}-pyrene are best fit with biexponential decay kinetics. The biexponential nature of these decays is most likely the result d^{10}-pyrene aggregation due to the observation of broad, structure less emission in β-estradiol molecular glasses containing 5 wt.% d^{10}-pyrene.

Experimental

Materials

β-Estradiol (98%), cholesterol (99%), β-sitosterol (70%), Bis(2,4-difluorophenylpyridinato)-tetrakis(1-pyrazolyl)borate iridium(III) (i.e., FIr6), and d^{10}-pyrene (>99.0%; >98 atom% D) were purchased from Sigma-Aldrich and used as received. Lithocholic acid (95%) was purchased from Cayman Chemical Company and used as received. All biologically sourced materials were stored at −20 °C.

Thermal Analysis

A TA Instruments Q5000 Thermogravimetric Analyzer (TGA) was used to set the temperature bounds for DSC analysis to ensure no more than 2 wt.% of the sample was lost due to thermal decomposition. A TA Instruments DSC 2500 with a refrigerated water cooler (TA RSC90) was used to determine the primary and secondary phase transitions of all samples. Materials were prepared

in hermetically sealed aluminum sample pans (T190415, T190221) with a pinhole to allow the release of residual moisture from the sample during heating cycles. Heating cycles were conducted with a ramp rate of 20 °C/min, the samples were subsequently quenched at a rate of 20 °C/min before a second heating/cooling cycle was conducted at a rate of 10 °C/min, respectively. A rapid cooling rate was chosen to mimic thermal quenching required during thin film casting. The effect of cooling rate on the fictive temperature has been previously described.[9] Host materials were analyzed neat and with various loadings of anthracene to determine a threshold for maximum doping tolerance.

X-Ray Scattering Measurements

Wide Angle X-ray Scattering (WAXS) measurements were conducted using a Xenocs Xuess 3.0 laboratory beamline with a microfocus sealed tube Cu source (30 W/30 μm) and a Pilatus 300 K hybrid photon counting detector to collect the 2D diffraction patterns. WAXS diffraction patterns were collected with the sample positioned at a distance of 0.055 mm from the detector over a time period of 60 seconds. For temperature dependent measurements the sample was mounted onto a high temperature sample stage and heated at a rate of 5 °C/minute until the desired temperature was reached and held constant during the WAXS measurements. WAXS diffraction data was analyzed and plotted using Origin 2018b 64bit software.

Optical Microscopy

Optical microscopy was performed using a Keyence VHX-100 Digital Microscope. The β-estradiol molecular glass was heated on a Mettler FP82HT heating stage controlled by a Mettler FP90 central processor.

Preparation of Molecular Glass Thin-Films for Photophysical Characterization

β-estradiol and lithocholic acid thin-films containing 5 wt.% d^{10}-pyrene and 1 wt.% FIr6 and 5 wt.% d^{10}-pyrene were cast for photophysical characterization. Mixtures were prepared in an aluminum pan and directly transferred to a hot plate set to 200 °C. The mixture was continuously stirred until a complete homogenous liquid was achieved. The aluminum pan was then removed from the hot plate and quenched to room temperature. This is repeated twice more, after which the mixture is scraped out and distributed onto a glass substrate. The open-faced film is then capped with a second clean glass slide and transferred onto a hotplate set to 10 °C above the melting temperature of the host material. The top slide is depressed using a pair of forceps, ensuring complete thermal contact is made with the surface of the hot plate. The forceps are removed from the top slide once there is evidence that the pressure from the top slide is enough to move the melted liquid within the film. The melted film is allowed to sit on the surface of the hotplate while bubbles form and migrate to the edge of the glass or combine forming larger bubbles. The film is then transferred to an aluminum block at room temperature and forceps are used to depress the top slide, pushing out bubbles while the film rapidly cools. Photos depicting the thin-film melt process are shown in Figures S7.

Thin-Film Thickness

Film thickness was measured using a Mitutoyo digital indicator (Mitutoyo ID-C125EXB) with a spindle lifting cable, relative to a flat surface. The deviation across a thin film was recorded by measuring four corners of a thin film coupon. The digital indicator used to measure film thickness has an accuracy of 2.54 μm. The box-and-whisker plot in Figure S9 was generated by measuring the thickness of β-estradiol and lithocholic acid thin films in 4 positions.

Photophysical characterization

Ground state absorption measurements were acquired using a Cary 5000 Series UV-Vis spectrometer. Steady-state phosphorescence spectra and phosphorescence lifetime measurements were collected using a Xe flashlamp and a gated PMT detector. The glass slides were placed in a solid sample holder at a 45° angle relative to the excitation source and the detector. The luminescence signal emitted from the front-face of the sample was collected. It should be noted that both the steady-state and time-resolved phosphorescence data were collected using a gate delay on the luminescence detector. This is necessary due to the dual luminescent behavior of d^{10}-pyrene in these materials under steady-state irradiation. The gate delay allows for the resolution of the phosphorescence signal without interference of the fluorescence signal. This also diminished the amount of scatter on the detector due to the front face geometry used in data collection. Gated phosphorescence spectra were collected with a lamp frequency of 10 Hz, a gate delay of 20 μs, and a gate width of 99 μs. Gated luminescence lifetimes were collected using a lamp frequency of 0.1 Hz, a gate delay of 20 μs, and a gate width of 9999 μs. Phosphorescence spectra of neat d^{10}-pyrene in β-estradiol and lithocholic acid molecular glasses were excited at 355 nm. The luminescence intensity was collected from 550–800 nm using a 1 nm step size. The excitation bandwidth was 3.00 nm and the emission bandwidth was 0.90 nm. Phosphorescence spectra of the FIr6 and d^{10}-pyrene donor-acceptor pair in β-estradiol and lithocholic acid molecular glasses were excited at 405 nm. The luminescence intensity was collected from 550–800 nm using a 1 nm step size. The excitation bandwidth was 3.00 nm and the emission bandwidth was 0.90 nm. The luminescence lifetime decays collected from all four samples were fit best using biexponential decays. Fit details and pre-exponential analysis are provided in Table S3.

Phosphorescence quantum yields were determined using an Edinburgh Instruments FLS980 spectrometer equipped with an integrating sphere capable of measuring solid samples. All samples were excited at 355 nm. The excitation intensity was set using a blank consisting of two 1 cm by 1 cm glass slides placed on the solid sample holder inside the sphere. The emission slit width was set to 4.5 mm and the excitation slit width was set to 0.4 mm to obtain approximately one million counts on the detector at the wavelength of excitation. Spectra were collected from 340–800 nm with a 1 nm step size and a dwell time of 0.5 s and each spectrum was repeated three times. The amount of light absorbed was determined by taking the difference of the integrated excitation signals of the blank and the sample spectra. Phosphorescence quantum yield was then determined integrating the samples above 575 nm to minimize any fluorescence emission.

Supporting Information

Thermogravimetric analysis of neat steroidal host materials, T_g, T_m, and $\Delta H(T_m)$ values for neat steroidal host materials and host-guest formulations containing d^{10}-pyrene and FIr6 with d^{10}-pyrene, DSC data for d^{10}-pyrene and host-guest formulations of lithocholic acid and β-estradiol with d^{10}-pyrene and

FIr6 with d^{10}-pyrene, thin-film processing details, thin-film thickness measurements, UV-vis absorption spectra of lithocholic acid and β-estradiol containing FIr6 with d^{10}-pyrene, and luminescence lifetime decay analysis of lithocholic acid and β-Estradiol thin-films containing d^{10}-pyrene and FIr6 with d^{10}-pyrene.

Acknowledgements

All AFRL affiliated authors recognize the Air Force Office of Scientific Research under AFOSR Award 9550-19-1-18RX056 and the Air Force Research Laboratory/RXAP contract FA8650-16-D-5402-0001. Some parts of this manuscript were previously posted online as part of the Master of Science thesis of author J. J. Flynn.[47]

Conflict of Interest

The authors declare no conflict of interest.

Data Availability Statement

The data that support the findings of this study are available from the corresponding author upon reasonable request.

Keywords: differential scanning calorimetry · host-guest systems · molecular glass · room-temperature phosphorescence · wide angle X-ray scattering

[1] Kenry, C. Chen, B. Liu, *Nat. Commun.* **2019**, *10*, 2111.
[2] S. Hirata, *Adv. Opt. Mater.* **2017**, *5*, 1700116.
[3] Y. Liu, G. Zhan, Z.-W. Liu, Z.-Q. Bian, C.-H. Huang, *Chin. Chem. Lett.* **2016**, *27*, 1231–1240.
[4] Z. Wu, J. Nitsch, T. B. Marder, *Adv. Opt. Mater.* **2021**, *9*, 2100411.
[5] H. Ma, A. Lv, L. Fu, S. Wang, Z. An, H. Shi, W. Huang, *Ann. Phys.* **2019**, *531*, 1800482.
[6] W. Zhao, Z. He, B. Z. Tang, *Nat. Rev. Mater.* **2020**, *5*, 869–885.
[7] J. Guo, C. Yang, Y. Zhao, *Acc. Chem. Res.* **2022**, *55*, 1160–1170.
[8] Y. Gong, J. Yang, M. Fang, Z. Li, *Cell Reports Phys. Sci.* **2021**, *3*, 100663.
[9] X. Yan, H. Peng, Y. Xiang, J. Wang, L. Yu, Y. Tao, H. Li, W. Huang, R. Chen, *Small* **2022**, *18*, 2104073.
[10] W. Wang, Y. Zhang, W. J. Jin, *Coord. Chem. Rev.* **2020**, *404*, 213107.
[11] L. Xiao, H. Fu, *Chem. A Eur. J.* **2019**, *25*, 714–723.
[12] M. Singh, K. Liu, S. Qu, H. Ma, H. Shi, Z. An, W. Huang, *Adv. Opt. Mater.* **2021**, *9*, 2002197.
[13] H.-R. Wang, X.-G. Yang, J.-H. Qin, L.-F. Ma, *Inorg. Chem. Front.* **2021**, *8*, 1942–1950.
[14] M. A. Baldo, S. Lamansky, P. E. Burrows, M. E. Thompson, S. R. Forrest, *Appl. Phys. Lett.* **1999**, *75*, DOI 10.1063/1.124258.
[15] N. J. Turro, *Modern Molecular Photochemistry*, University Science Books, **1991**.
[16] S. Hirata, K. Totani, J. Zhang, T. Yamashita, H. Kaji, S. R. Marder, T. Watanabe, C. Adachi, *Adv. Funct. Mater.* **2013**, *23*, 3386–3397.
[17] S. Hirata, M. Vacha, *Adv. Opt. Mater.* **2017**, *5*, 1–11.
[18] M. Stähelin, D. M. Burland, M. Ebert, R. D. Miller, B. A. Smith, R. J. Twieg, W. Volksen, C. A. Walsh, *Appl. Phys. Lett.* **1992**, *61*, 1626–1628.
[19] M. Louis, H. Thomas, M. Gmelch, F. Fries, A. Haft, J. Lindenthal, S. Reineke, *Adv. Opt. Mater.* **2020**, *8*, 2000427.
[20] M. Louis, H. Thomas, M. Gmelch, A. Haft, F. Fries, S. Reineke, *Adv. Mater.* **2019**, *31*, 1807887.
[21] S. Scypinski, L. J. C. Love, *Anal. Chem.* **1984**, *56*, 322–327.
[22] D. Li, F. Lu, J. Wang, W. Hu, X. M. Cao, X. Ma, H. Tian, *J. Am. Chem. Soc.* **2018**, *140*, 1916–1923.
[23] T. Ogoshi, Y. Chujo, *Macromolecules* **2003**, *36*, 654–660.
[24] C. Marquez, F. Huang, W. M. Nau, *IEEE Trans. Nanobioscience* **2004**, *3*, 39–45.
[25] W. L. Mock, N. Y. Shih, *J. Org. Chem.* **1986**, *51*, 4440–4446.
[26] J. W. Lee, S. Samal, N. Selvapalam, H. J. Kim, K. Kim, *Acc. Chem. Res.* **2003**, *36*, 621–630.
[27] J. Lagona, P. Mukhopadhyay, S. Chakrabarti, L. Isaacs, *Angew. Chem. Int. Ed.* **2005**, *44*, 4844–4870; *Angew. Chem.* **2005**, *117*, 4922–4949.
[28] A. Koc, D. Tuncel, *Isr. J. Chem.* **2018**, *58*, 334–342.
[29] K. Miki, A. Masui, N. Kasai, M. Miyata, M. Shibakami, K. Takemoto, *J. Am. Chem. Soc.* **1988**, *110*, 6594–6596.
[30] M. Miyata, N. Tohnai, I. Hisaki, *Acc. Chem. Res.* **2007**, *40*, 694–702.
[31] Y. Katsurada, S. Hirata, K. Totani, T. Watanabe, M. Vacha, *Adv. Opt. Mater.* **2015**, *3*, 1726–1737.
[32] S. Hirata, *J. Mater. Chem. C* **2018**, *6*, 11785–11794.
[33] K. Narushima, Y. Kiyota, T. Mori, S. Hirata, M. Vacha, *Adv. Mater.* **2019**, *31*, 1807268.
[34] S. Hirata, K. Totani, T. Watanabe, H. Kaji, M. Vacha, *Chem. Phys. Lett.* **2014**, *591*, 119–125.
[35] S. Hirata, K. Totani, T. Yamashita, C. Adachi, M. Vacha, *Nat. Mater.* **2014**, *13*, 938–946.
[36] A. Qin, B. Z. Tang, *Nat. Mater.* **2014**, *13*, 917–918.
[37] S. Hirata, M. Vacha, *J. Phys. Chem. Lett.* **2017**, *8*, 3683–3689.
[38] S. Hirata, M. Vacha, *Adv. Opt. Mater.* **2016**, *4*, 297–305.
[39] S. Hirata, M. Vacha, *J. Phys. Chem. Lett.* **2016**, *7*, 1539–1545.
[40] D. Mahlin, S. Ponnambalam, M. Heidarian Höckerfelt, C. A. S. Bergström, *Mol. Pharm.* **2011**, *8*, 498–506.
[41] D. Mahlin, C. A. S. Bergström, *Eur. J. Pharm. Sci.* **2013**, *49*, 323–332.
[42] K. Kawakami, *Pharmaceutica* **2019**, *11*, 202.
[43] E. Hendrickx, B. L. Volodin, D. D. Steele, J. L. Maldonado, J. F. Wang, B. Kippelen, N. Peyghambarian, *Appl. Phys. Lett.* **1997**, *71*, 1159–1161.
[44] S. K. Yesodha, C. K. Sadashiva Pillai, N. Tsutsumi, *Prog. Polym. Sci.* **2004**, *29*, 45–74.
[45] J. Mei, N. L. C. Leung, R. T. K. Kwok, J. W. Y. Lam, B. Z. Tang, *Chem. Rev.* **2015**, *115*, 11718–11940.
[46] J. Mei, Y. Hong, J. W. Y. Lam, A. Qin, Y. Tang, B. Z. Tang, *Adv. Mater.* **2014**, *26*, 5429–5479.
[47] Some parts of this manuscript were previously posted online as part of the Master of Science thesis of author J. J. Flynn: J. J. Flynn, Master of Science Thesis, University of Dayton, **2020**. http://rave.ohiolink.edu/etdc/view?acc_num=dayton1588192751503223.
[48] Q. Zheng, Y. Zhang, M. Montazerian, O. Gulbiten, J. C. Mauro, E. D. Zanotto, Y. Yue, *Chem. Rev.* **2019**, *119*, 7848–7939.
[49] Y. Tsubomoto, S. Hirata, K. Totani, M. Vacha, T. Watanabe, *J. Photopolym. Sci. Technol.* **2015**, *28*, 573–577.
[50] J. A. Baird, B. Van Eerdenbrugh, L. S. Taylor, *J. Pharm. Sci.* **2010**, *99*, 3787–3806.
[51] E. L. Stevenson, R. W. Lancaster, A. B. M. Buanz, L. S. Price, D. A. Tocher, S. L. Price, *CrystEngComm* **2019**, *21*, 2154–2163.
[52] J. Langelaar, R. P. H. Rettschnick, G. J. Hoijtink, *J. Chem. Phys.* **1971**, *54*, 1–7.
[53] S. R. Aubuchon, *TA334 – Intrepretation of the Crystallization Peak of Supercooled Liquids Using Tzero DSC*, New Castle, DE **2007**.
[54] O. A. Khakhel', *J. Appl. Spectrosc.* **2001**, *68*, 280–286.
[55] M. M. Islam, Z. Hu, Q. Wang, C. Redshaw, X. Feng, *Mater. Chem. Front.* **2019**, *3*, 762–781.

Manuscript received: May 12, 2022
Revised manuscript received: August 19, 2022
Accepted manuscript online: August 22, 2022
Version of record online: September 26, 2022